Inorg. Chem. **2004**, *43*, 2914–2921

Solvothermal Syntheses, Crystal Structures, and Thermal Properties of New Manganese Thioantimonates(III): The First Example of the Thermal Transformation of an Amine-Rich Thioantimonate into an Amine-Poorer Thioantimonate

Michael Schaefer, Christian Näther, Nicolai Lehnert, and Wolfgang Bensch*

Institut für Anorganische Chemie der Christian-Albrechts Universität Kiel, Olshausenstrasse 40, D-24098 Kiel, Germany

Received August 15, 2003

Two new neutral thioantimonates(III) were first prepared by the reaction of elemental manganese, antimony, and sulfur in tren (tren = tris(2-aminoethyl)amine, $C_6H_{18}N_4$) at 140 °C. In the amine-rich compound $[Mn(tren)]_2Sb_2S_5$ (**1**) the trigonal SbS_3 pyramids are connected via common corners (S(3)) into the tetradentate $[Sb_2S_5]^{4-}$ anion. Four S atoms have bonds to the manganese atoms of the $[Mn(tren)^{2+}]$ cations. A special structural feature is the large Sb–S(3)–Sb(a) angle of 134°. Density functional calculations clearly demonstrate that this large angle results from the steric interactions between the two Mn(tren) subunits. In the crystal structure of the amine-poorer compound $[Mn(tren)]_2Mn_2Sb_4S_{10}$ (**2**), MnS_4 tetrahedra and SbS_3 pyramids are linked via common corners and edges to form a new heterometallic $[Mn_2Sb_4S_{10}]$ core. The $[Mn(C_6H_{18}N_4)^{2+}]$ cations are located at the periphery of the core and are bound to the $[Mn_2Sb_4S_{10}]$ unit via two S atoms. The thermal behavior of both compounds was investigated using simultaneous thermogravimetry (TG), differential thermoanalysis, and mass spectroscopy. The amine-richer compound **1** decomposes in three steps upon heating. After the first TG step an intermediate phase is formed, which was identified as the amine-poorer compound **2** by X-ray diffraction. Reaction of compound **2** at 140 °C with an excess of tren forms the amine-rich compound **1**.

Introduction

The solvothermal syntheses of chalcogenidometalates in the presence of amines as structure-directing molecules has become of increasing interest. One major goal in this field is the development of strategies for a more rational construction of their structures to prepare new compounds such as, e.g., open framework chalcogenidometalates with organic molecules acting as space fillers and/or charge balancing ions or condensed frameworks with interesting physical properties. Open frameworks should exhibit dramatically different physical and chemical properties compared to the well-established oxidic counterparts. Many thio and seleno compounds with interesting structural features were prepared during the past decade,[1−14] but in all cases the structure-directing molecules could not be removed without a collapse of the materials. Such a removal of the structure-directing amines is a prerequisite for the preparation of porous compounds with accessible empty space. On the other hand, the emission of the structure-directing molecules may lead to a rearrangement of the building units, forming materials with a higher degree of condensation. A few years ago we started to prepare new chalgogenidometalates on the basis

* Author to whom correspondence should be addressed. Fax: +49 (0)-431/880-1520. E-mail: wbensch@ac.uni-kiel.de.

(1) Sheldrick, W. S.; Wachhold, M. *Angew. Chem.* **1997**, *109*, 214.
(2) Sheldrick, W. S.; Wachhold, M. *Coord. Chem. Rev.* **1998**, *176*, 211.
(3) Sheldrick, W. S. *J. Chem. Soc., Dalton Trans.* **2000**, 3041.
(4) Wang, X.; Jacobson, A. J.; Liebau, F. *J. Solid State Chem.* **1998**, *140*, 387.
(5) Ko, Y.; Tan, K.; Nellis, D. M.; Koch, S.; Parise, J. B. *J. Solid State Chem.* **1995**, *114*, 506.
(6) Tan, K.; Ko, Y.; Parise, J. B.; Darovsky, A. *Chem. Mater.* **1996**, *8*, 493.
(7) Parise, J. B.; Tan, K. *Chem. Commun.* **1996**, 1687.
(8) Cahill, C. L.; Parise, J. B. *Chem. Mater.* **1997**, *9*, 807.
(9) Cahill, C. L.; Gugliotta, B.; Parise, J. B. *Chem. Commun.* **1998**, 1715.
(10) Cahill, C. L.; Ko, Y.; Parise, J. B. *Chem. Mater.* **1998**, *10*, 19.
(11) Cahill, C. L.: Parise, J. B. *J. Chem. Soc., Dalton Trans.* **2000**, 1475.
(12) Li, H.; Eddaoudi, M.; Laine, A.; O'Keeffe, M.; Yaghi, O. M. *J. Am. Chem. Soc.* **1999**, *121*, 6096.
(13) Li, H.; Laine, A.; O'Keeffe, M.; Yaghi, O. M. *Science* **1999**, *283*, 1145.
(14) Li, H.; Kim, J.; Groy, T. L.; O'Keeffe, M.; Yaghi, O. M. *J. Am. Chem. Soc.* **2001**, *123*, 4867.

10.1021/ic034970+ CCC: $27.50 © 2004 American Chemical Society
Published on Web 03/30/2004

of antimony. Several primary SbS_x building blocks are known for such compounds which can be used for the construction of thioantimonate frameworks. In continuing work we started to investigate whether it is possible to incorporate transition-metal (TM) atoms into thioantimonate networks. The idea was to compensate the high negative charge of the thioantimonate anions by the TM ions, thus yielding charge neutral networks, and to alter the physical and chemical properties of such compounds to influence their optical and magnetic properties. According to this idea, we successfully synthesized a series of compounds with composition $Mn_2Sb_2S_5 \cdot L$ (L = 1,3-diaminopropane (dap), methylamine (ma), ethylamine (ea), ethylenediamine (en))[15,16] showing a layered structure with pores within the layers. But in most cases the usage of, e.g., bi- or tridentate amines as the solvents leads to the formation of isolated $TM(amine)_z^{n+}$ complexes.[17−20] Such complexes were found to act as suitable structure directors, but the TM^{n+} ions are not bound to the $Sb_xS_y^{m-}$ units and no frameworks are formed. Another idea was to alter the physical and chemical properties of thioantimonates by the integration of TM^{n+} ions into the framework, i.e., changing the optical and magnetic properties. But application of bi- or tridentate amines as the solvents[17−20] often formed isolated $TM(amine)_z^{n+}$ complexes. Such complexes were found to act as suitable structure directors, but the TM^{n+} ions are not bound to the $Sb_xS_y^{m-}$ units. Very recently we demonstrated that TM^{n+} ions can be integrated into thioantimonate frameworks using an amine such as tren (tren = tris(2-aminoethyl)amine) which leaves one or two coordination sites free at the TM^{n+} ions, enabling bond formation to the Sb_xS_y network.[21,22] For instance, $[Fe(tren)]FeSbS_4$ is a mixed-valent compound.[23] The Fe^{3+} ion is part of a protein analogous $[2Fe^{III}-2S]$ cluster encapsulated within the thioantimonate anion, whereas the $Fe(tren)^{2+}$ cation has one bond to a S atom of the anion. Other exciting examples for the successful incorporation of TM^{n+} ions are $[Co(tren)]Sb_2S_4$ and $[Ni(tren)]Sb_2S_4$.[24] In $[Co(tren)]Sb_2S_4$ a two-dimensional thioantimonate(III) network is found with different Sb_xS_x rings. The $Co(tren)^{2+}$ cations are bound to the anion via one S atom and are located in the cavities of $Sb_{10}S_{10}$ rings. In $[Ni(tren)]Sb_2S_4$ the SbS_3 pyramids are interconnected to form a one-dimensional thioantimonate(III) chain. The $Ni(tren)^{2+}$ cations have bonds to two S atoms of the anion, yielding a $NiSb_2S_3$ heteroring. During our systematical exploration of the Mn−Sb−S−tren system, we synthesized the two title compounds $[Mn(tren)]_2Sb_2S_5$ (**1**) and $[Mn(tren)]_2Mn_2Sb_4S_{10}$ (**2**). Formally, compound **1** can be regarded as amine-rich and **2** as an amine-poor sample. Following the ideas of Näther et al.,[25−28] compound **1** was thermally decomposed in a directed way to form compound **2**. This is the first example in thioantimonate(III) chemistry showing that thermal decomposition reactions are a promising technique for the synthesis of new compounds. The reaction is of special interest because the degree of condensation increases on going from compound **1** to compound **2** and offers a synthetic approach for the modification of chalcogenidometalate frameworks. In addition, the solvothermal syntheses of chalcogenidometalates are normally performed using the elements as starting materials and an excess of amines. Very often mixtures of different compounds are obtained, and the synthesis of metal-rich compounds is difficult to achieve. In such cases thermal decomposition reactions can be an alternative tool for the preparation of large amounts of new compounds which cannot be prepared in solution or which are always obtained as mixtures. Furthermore, the reverse reaction from **2** to **1** was also successful, demonstrating that even complex compounds can be used as starting materials for the synthesis of thioantimonates(III). In compound **1** an unusual large angle around a S atom joining two Sb centers of 134° is observed. Density functional calculations are performed to gain insight into whether electronic or sterical effects are responsible for the enlarged angle. In the present paper we report the syntheses, crystal structures, and thermal reactions of the two new manganese thioantimonates(III). The results of the theoretical calculations undertaken for compound **1** are also presented.

Experimental Section

Synthesis of 1. Orange-colored plates of $[Mn(tren)]_2Sb_2S_5$ were synthesized using elemental Mn (54.9 mg, 1 mmol), Sb (121.76 mg, 1 mmol), and S (80 mg, 2.5 mmol) in 95% tren (5 mL, 33.4 mmol). The mixture was heated to 140 °C for 7 days in a Teflon-lined steel autoclave with an inner volume of approximately 30 mL and cooled within 3 h to room temperature. The product was filtered off, washed with acetone, and stored under vacuum. The yield based on Mn is about 60%. As byproducts $[Mn(tren)(trenH)]SbS_4$[21] and crystalline Sb were identified by X-ray diffraction (XRD). C, H, N, S Anal. Found for selected crystals: C, 17.2; H, 4.4; N, 13.2; S, 18.0. Calcd: C, 17.9; H, 4.5; N, 13.9; S, 19.9.

Synthesis of 2. $[Mn(tren)]_2Mn_2Sb_4S_{10}$ was obtained from elemental Mn (54.9 mg, 1 mmol), Sb (121.76 mg, 1 mmol), and S (80 mg, 2.5 mmol) in an aqueous solution of 40% tren (5 mL, 13.4 mmol) at 140 °C in a Teflon-lined steel autoclave (∼30 mL). After 7 days the mixture was cooled within 3 h to room temperature, and the orange-colored squares were filtered off, washed with acetone, and stored under vacuum. The yield based on Mn is about 80%. Besides the title compound an unknown amorphous phase and crystalline Sb were observed by XRD. C, H, N, S Anal. Found for selected crystals: C, 10.8; H, 2.8; N, 8.4; S, 23.6. Calcd: C, 10.9; H, 2.8; N, 8.5; S, 24.3.

Crystal Structure Determination. All data were collected using an imaging plate diffraction system (IPDS) from Stoe & Cie

(15) Bensch, W.; Schur, M. *Eur. J. Solid State Inorg. Chem.* **1996**, *33*, 1149.
(16) Schur, M.; Bensch, W. *Z. Naturforsch.* **2002**, *57b*, 1.
(17) Bensch, W.; Näther, C.; Stähler, R. *Chem. Commun.* **2001**, 477.
(18) Stähler, R.; Näther, C.; Bensch, W. *Eur. J. Inorg. Chem.* **2001**, 1835.
(19) Stähler, R.; Bensch, W. *Z. Anorg. Allg. Chem.* **2002**, *628*, 1657.
(20) Stähler, R.; Näther, C.; Bensch, W. *Acta Crystallogr., Sect. C* **2001**, *57*, 26.
(21) Schaefer, M.; Engelke, L.; Bensch, W. *Z. Anorg. Allg. Chem.* **2003**, *629*, 1912.
(22) Schaefer, M.; Bensch, W. *Solid State Sci.* **2003**, *5*, 1135.
(23) Kiebach, R.; Bensch, W.; Hoffmann, R.-D.; Pöttgen, R. *Z. Anorg. Allg. Chem.* **2003**, *629*, 532.
(24) Stähler, R.; Bensch, W. *Eur. J. Inorg. Chem.* **2001**, 3073.
(25) Näther, C.; Wriedt, C. M.; Jess, I. *Z. Anorg. Allg. Chem.* **2002**, *628*, 394.
(26) Näther, C.; Jess, I.; Studzinski, H. *Z. Naturforsch.* **2001**, *56b*, 997.
(27) Näther, C.; Jess, I. *Monatsh. Chem.* **2002**, *132*, 897.
(28) Näther, C.; Jess, I. *J. Solid State Chem.* **2002**, *169*, 103.

Table 1. Crystallographic Data for **1** and **2**

	1	2
cryst syst	orthorhombic	triclinic
a/Å	8.6313(4)	8.420(2)
b/Å	18.988(1)	9.900(2)
c/Å	16.410(1)	11.430(2)
α/deg	90	101.11(3)
β/deg	90	105.27(3)
γ/deg	90	91.76(3)
V/Å^3	2689.5 (2)	898.6(3)
space group	*Pbcn*	$P\bar{1}$
T/°C	20	20
Z	8	1
density(calcd)/g cm^{-3}	1.991	2.439
μ/mm^{-1}	3.31	4.92
mol wt	403.08	1319.85
R1 for $F_o > 4\sigma(F_o)$[a]	0.0290	0.0202
wR2 for all reflns[b]	0.0726	0.0526

[a] $R1 = \sum||F_o| - |F_c|/\sum|F_o|$. [b] $wR2 = [\sum[w(F_o^2 - F_c^2)^2]/\sum[w(F_o^2)^2]]^{1/2}$.

(graphite-monochromated Mo Kα radiation, $\lambda = 0.71073$ Å). The measurements were carried out at 293 K. The structure solutions were performed using SHELXS-97.[29] The structure refinements were done against F^2 using SHELXL-97.[30] For compound **1** a numerical absorption correction was applied using X-Red[31] and X-Shape.[32] All non-hydrogen atoms were refined anisotropically. The hydrogen atoms were positioned with idealized geometry and refined with individual isotropic displacement parameters using the riding model. The crystals of compound **2** were always nonmerohedrically twinned, which was seen by the inspection of the reciprocal space using the program recipe from Stoe & Cie. The reflections of both individuals were indexed and integrated separately using the programs recipe and twin.[33] Crystal data and results of the structure refinement as well as selected bond lengths and angles are found in Tables 1 and 2.

Crystallographic data (excluding structure factors) for the structures reported in this paper have been deposited with the Cambridge Crystallographic Data Centre (CCDC) as Supplementary Publication Nos. CCDC 213776 (**1**) and CCDC 213777 (**2**). Copies of the data can be obtained free of charge on application to the CCDC, 12 Union Rd., Cambridge CB2 1 EZ, U.K. [fax, +44-(0)-1223−336033; e-mail, deposit@ccdc.cam.ac.uk].

X-ray Powder Diffraction. The X-ray powder patterns were recorded in transmission geometry using a Stoe Stadi-P diffractometer with a position-sensitive detector (PSD) (Cu Kα radiation, $\lambda = 1.540598$ Å).

Thermal Behavior. Differential thermal analysis (DTA)−thermogravimetry (TG)−mass spectrometry (MS) measurements were performed simultaneously using the STA-409CD with Skimmer coupling from Netzsch, which is equipped with a quadrupole mass spectrometer, QMA 400 (max 512 amu), from Balzers. The MS measurements were performed in analogue and trend scan mode. All measurements were corrected according to buoyancy and current effects and were performed using heating rates of 4 K/min in Al_2O_3 crucibles under a dynamic helium atmosphere (flow rate 75 mL/min, purity 4.6).

Table 2. Selected Bond Lengths (Å) and Angles (deg) for **1** and **2**[a]

		1	
Sb−S(1)	2.3980(8)	Sb−S(2)	2.3589(7)
Sb−S(3)	2.4725(5)	Mn−S(1)	2.5006(9)
Mn−S(2)	2.7036(8)	Mn−N(1)	2.334(3)
Mn−N(2)	2.250(3)	Mn−N(3)	2.280(3)
Mn−N(4)	2.341(3)		
Sb−S(3)−Sb[b]	134.06(5)	S(1)−Sb−S(2)	98.07(3)
S(1)−Sb−S(3)	102.90(2)	S(2)−Sb−S(3)	107.79(3)
N(1)−Mn−S(1)	173.82(8)	N(1)−Mn−S(2)	98.97(8)
N(2)−Mn−S(1)	104.29(8)	N(2)−Mn−S(2)	86.33(7)
N(3)−Mn−S(1)	105.52(8)	N(3)−Mn−S(2)	86.37(7)
N(4)−Mn−S(1)	97.97(8)	N(4)−Mn−S(2)	174.07(8)
		2	
Sb(1)−S(1)	2.3962(9)	Sb(1)−S(2)	2.4196(8)
Sb(1)−S(3)	2.4831(9)	Sb(2)−S(3)	2.4673(9)
Sb(2)−S(4)	2.466(1)	Sb(2)−S(5)	2.365(1)
Mn(1)−S(1)	2.4805(9)	Mn(1)−S(2)	2.836(1)
Mn(2)−S(2)	2.4693(9)	Mn(2)−S(4)	2.569(1)
Mn(2)−S(4)[c]	2.4953(9)	Mn(2)−S(5)	2.478(1)
Mn(1)−N(1)	2.326(2)	Mn(1)−N(2)	2.243(2)
Mn(1)−N(3)	2.269(2)	Mn(1)−N(4)	2.284(3)
	Long Sb−S Bonds		
Sb(1)−Sb(2)[d]	3.565(1)	Sb(1)−S(4)[d]	3.676(1)
Sb(2)−S(2)[d]	3.897(2)		
Sb(1)−S(3)−Sb(2)	108.17(4)	S(1)−Sb(1)−S(2)	97.19(4)
S(1)−Sb(1)−S(3)	92.72(4)	S(2)−Sb(1)−S(3)	91.73(4)
S(3)−Sb(2)−S(4)	95.87(4)	S(3)−Sb(2)−S(5)	94.26(4)
S(4)−Sb(2)−S(5)	94.17(4)	Mn(1)−S(2)−Mn(2)	114.53(4)
N(1)−Mn(1)−S(1)	173.47(7)	N(1)−Mn(1)−S(2)	99.52(8)
N(2)−Mn(1)−S(1)	100.69(7)	N(2)−Mn(1)−S(2)	83.03(7)
N(3)−Mn(1)−S(1)	107.86(7)	N(3)−Mn(1)−S(2)	87.70(8)
N(4)−Mn(1)−S(1)	97.04(8)	N(4)−Mn(1)−S(2)	175.84(8)

[a] Estimated standard deviations are given in parentheses. [b] Symmetry code $1 - x, y, 0.5 - z$. [c] Symmetry code $2 - x, 1 - y, 1 - z$. [d] Symmetry code $1 - x, 1 - y, 1 - z$.

Elemental Analysis. These investigations were performed using a EuroEA elemental analyzer from Eurovector.

Density Functional Calculations. Spin-unrestricted density functional theory (DFT) calculations using Becke's three-parameter hybrid functional with the correlation functional of Lee, Yang, and Parr (B3LYP)[34] were performed with the program package Gaussian 98.[35] The applied LanL2DZ basis set uses Dunning/Huzinaga full double-ζ (D95)[36] basis functions on first-row and Los Alamos effective core potentials plus double-ζ (DZ) functions on all other atoms.[37] The structure of the discrete dimer $[Mn(tren)]_2Sb_2S_5$ (cf. Figure 1) was fully optimized in C_1 symmetry. The higher symmetry

(29) Sheldrick, G. M. *SHELXS-97, Program for Crystal Structure Determination*; University of Göttingen: Göttingen, Germany, 1997.
(30) Sheldrick, G. M. *SHELXL-97, Program for Crystal Structure Refinement*; University of Göttingen: Göttingen, Germany, 1997.
(31) Stoe & Cie. *X-Red32 V 1.11 Software*; Stoe & Cie GmbH: Darmstadt, Germany, 1998.
(32) Stoe & Cie. *X-Shape V 1.03 Software*; Stoe & Cie GmbH: Darmstadt, Germany, 1998.
(33) Stoe & Cie. *IPDS Program Package*, V. 2.89; Stoe & Cie GmbH: Darmstadt, Germany, 1998.
(34) (a) Becke, A. D. *Phys. Rev. A* **1988**, *38*, 3098. (b) Becke, A. D. *J. Chem. Phys.* **1993**, *98*, 1372. (c) Becke, A. D. *J. Chem. Phys.* **1993**, *98*, 5648.
(35) Frisch, M. J.; Trucks, G. W.; Schlegel, H. B.; Scuseria, G. E.; Robb, M. A.; Cheeseman, J. R.; Zakrzewski, V. G.; Montgomery, J. A., Jr.; Stratmann, R. E.; Burant, J. C.; Dapprich, S.; Millam, J. M.; Daniels, A. D.; Kudin, K. N.; Strain, M. C.; Farkas, O.; Tomasi, J.; Barone, V.; Cossi, M.; Cammi, R.; Mennucci, B.; Pomelli, C.; Adamo, C.; Clifford, S.; Ochterski, J.; Petersson, G. A.; Ayala, P. Y.; Cui, Q.; Morokuma, K.; Malick, D. K.; Rabuck, A. D.; Raghavachari, K.; Foresman, J. B.; Cioslowski, J.; Ortiz, J. V.; Stefanov, B. B.; Liu, G.; Liashenko, A.; Piskorz, P.; Komaromi, I.; Gomperts, R.; Martin, R. L.; Fox, D. J.; Keith, T.; Al-Laham, M. A.; Peng, C. Y.; Nanayakkara, A.; Gonzalez, C.; Challacombe, M.; Gill, P. M. W.; Johnson, B. G.; Chen, W.; Wong, M. W.; Andres, J. L.; Head-Gordon, M.; Replogle, E. S.; Pople, J. A. *Gaussian 98*, revision A.11; Gaussian, Inc.: Pittsburgh, PA, 1998.
(36) Dunning, T. H., Jr., Hay, P. J., Schaefer, H. F., III, Eds.; Plenum: New York, 1976.
(37) (a) Hay, P. J.; Wadt, W. R. *J. Chem. Phys.* **1985**, *82*, 270, 299. (b) Wadt, W. R.; Hay, P. J. *J. Chem. Phys.* **1985**, *82*, 284.

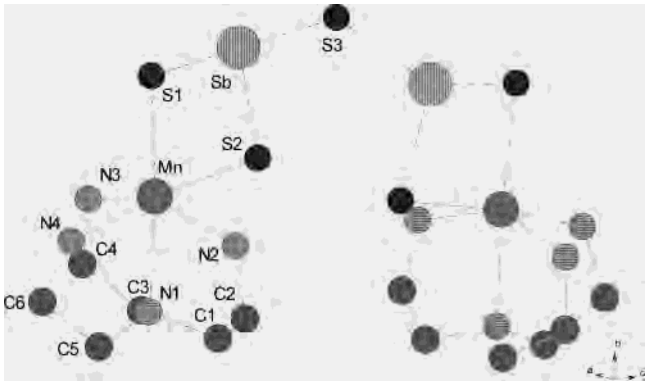

Figure 1. Crystal structure of **1** with labeling. Hydrogen atoms are omitted for clarity.

of the crystal structure has not been used in the calculations to fully explore the geometric flexibility of the dimer independent of crystal packing effects, etc. As described in the Results and Discussion, this leads to slight distortions which are due to the formation of extra hydrogen bonds in the gas phase, but no severe changes of the overall structure occur. From experiment it is known that the magnetic interaction between the two high-spin Mn^{2+} ions (both $S = 5/2$) through the $[Sb_2S_5]^{4-}$ bridge is weak. For the calculations, the ferromagnetical coupling scheme giving rise to a total spin of $S = 5$ for the dimer has been used. The calculated second derivatives show that the optimized structure represents a global minimum. Restricted potential energy surface (PES) scans along the Sb−S−Sb angle, where S is the central bridging sulfur, have also been performed with B3LYP/LanL2DZ for both the X-ray- and the DFT-optimized structures. In addition, the dependence of the above-mentioned Sb−S−Sb angle on the bulkiness of the coordinated fragment (here Mn(tren)) has been studied. Accordingly, structures have been calculated for the anion $[Sb_2S_5]^{4-}$ as well as the hypothetical models $[(Ni(NH_3)_2]_2Sb_2S_5$ and $[Ni(tma)_2]_2Sb_2S_5$ (tma = trimethylamine) with sterically less demanding metal(ligand) units bound to $[Sb_2S_5]^{4-}$. These calculations have been performed in C_1 symmetry using B3LYP/LanL2DZ. Nickel(II) was chosen in these calculations, because it has a lower coordination number than Mn(II) and it has a closed-shell ($S = 0$) electron configuration. The obtained structures of the $[Sb_2S_5]^{4-}$ unit in the Ni(II)−ammonia and the Ni(II)−tma complexes are comparable to that of $[Mn(tren)]_2Sb_2S_5$, whereas $[Sb_2S_5]^{4-}$ itself has a linear structure due to the strong Coulomb repulsion of the terminal negative charges.

Results and Discussion

The amine-rich compound $[Mn(tren)]_2Sb_2S_5$ (**1**) crystallizes in the orthorhombic space group *Pbcn* with eight formula units in the unit cell. The crystallographically independent manganese atom is surrounded by four nitrogen atoms of the tren ligand and two sulfur atoms of the anion within a distorted octahedron, MnN_4S_2 (Figure 1 and Table 2). The Mn(tren) complex and its derivatives have been known and studied for a long time, and some transition metal compounds were synthesized in the past.[38−40] The Sb atom has short bonds to three S atoms, forming the well-known SbS_3 trigonal pyramid.[15−20,22−24,41−51] The S(3) atom is located on a 2-fold axis, and the two SbS_3 pyramids are connected via this S atom, forming the unusual tetradentate $[Sb_2S_5]^{4-}$ anion. We note that the $[Sb_2S_5]^{4-}$ anion was observed in only a few compounds,[15,16,51] but never acting in such a manner as a multidentate ligand. The other four S atoms of the anion are bound to the two Mn atoms, forming two four-membered $MnSbS_2$ rings which are almost coplanar to each other (mean deviation from least-squares plane 0.0331 Å, angle between the planes 0.8°). We note that four-membered $MnSbS_2$ rings are rare and only a few examples exist.[15,16,22,44]

The Mn−N bonds vary between 2.250(3) and 2.341(8) Å. The longer bonds are in *trans* positions to the Mn−S bonds. The Mn−S distances range from 2.5006(9) to 2.7036(8) Å. The S(1) atom is within the distorted rectangular plane of the octahedron, and the elongation of the Mn−S(1) bond is due to sterical requirements (Table 2, Figure 1). A shorter Mn−S(2) distance would lead to strong repulsive interactions between N(2)H2 and S(2), which is energetically not favorable.

The Sb−S distances between 2.3589(7) and 2.4725(5) Å are similar with the data for SbS_3 units reported in the literature. The S−Sb−S angles are in the typical range from 98.07(9)° to 107.79(3)°. A highly interesting feature of the anion is the very large Sb−S(3)−Sb(a) angle of 134.06(5)° (Figure 1). Normally, the angles around S atoms are in the range from 90° to 110°. A detailed analysis of the geometry demonstrates that an angle about S(3) which is in the typical range would bring the two Mn(tren) units too close together. We note that the actual geometry yields a short intramolecular H···S distance of 2.541(1) Å (N(2)H2···S(2a) angle 154.34°). The $[Mn(tren)]_2Sb_2S_5$ molecules are stacked onto each other along [100], and due to the glide plane the orientation of neighbored rods shows an up−down alternation along [001] (see Figure 2). Between adjacent molecules intermolecular H···S separations ranging from 2.582(1) to 3.018(1) Å indicate hydrogen bonding.

The amine-poorer compound $[Mn(tren)]_2Mn_2Sb_4S_{10}$ (**2**) crystallizes in the triclinic space group $P\bar{1}$ with one formula unit in the unit cell. Two crystallographically independent Mn, two Sb, and five S atoms are found (Figure 3 and Table 2). Mn(1) is coordinated by four N atoms of the tren ligand and two S atoms of the anion in a distorted octahedral environment, $Mn(1)N_4S_2$ (Figure 3). The Mn(2) atom is surrounded by four S atoms, forming a distorted tetrahedron,

(38) Sime, R. J.; Dodge, R. P.; Zalkin, A.; Templeton, D. H. *Inorg. Chem.* **1971**, *10*, 537.
(39) Ciampolini, M.; Nardi, N. *Inorg. Chem.* **1966**, *5*, 41.
(40) Ellermeier, J.; Bensch, W. *Transition Met. Chem. (Dordrecht, Neth.)* **2002**, *27*, 763.
(41) Wang, X.; Liebau, F. *J. Solid State Chem.* **1994**, *111*, 385.
(42) Powell, A. V.; Paniagua, R.; Vaqueiro, P.; Chippindale, A. M. *Chem. Mater.* **2002**, *14*, 1220.
(43) Powell, A. V.; Boissiere, S.; Chippindale, A. M. *J. Chem. Soc., Dalton Trans.* **2000**, 4192.
(44) Pfitzner, A.; Kurowski, D. *Z. Kristallogr.* **2000**, *215*, 373.
(45) Powell, A. V.; Boissière, S.; Chippindale, A. M. *Chem. Mater.* **2000**, *12*, 182.
(46) Sheldrick, W. S.; Häusler, H.-J. *Z. Anorg. Allg. Chem.* **1988**, *557*, 105.
(47) Oliver-Fourcade, J.; Izghouti, L.; Philippot, E. *Rev. Chim. Min.* **1981**, *18*, 207.
(48) Graf, H. A.; Schäfer, H. *Z. Naturforsch.* **1972**, *27b*, 735.
(49) Cordier, G.; Schäfer, H. *Rev. Chim. Min.* **1981**, *18*, 218.
(50) Dörrscheidt, W.; Schäfer, H. *Z. Naturforsch.* **1981**, *36b*, 410.
(51) Stähler, R.; Bensch, W. *J. Chem. Soc., Dalton Trans.* **2001**, 2518.

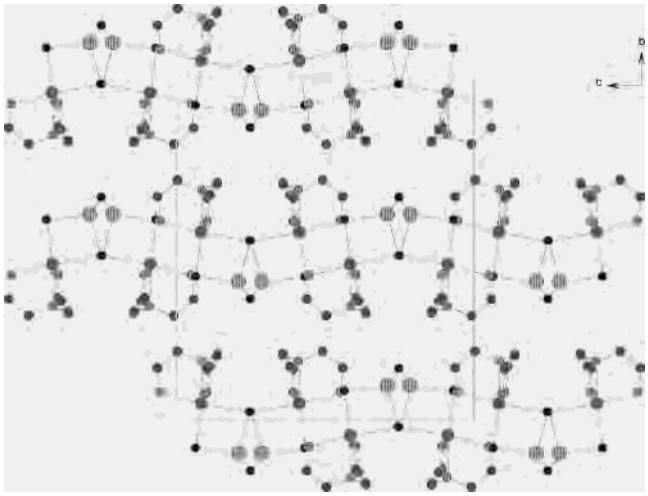

Figure 2. Arrangement of $[Mn(tren)]_2Sb_2S_5$ in the structure. H atoms are omitted for clarity.

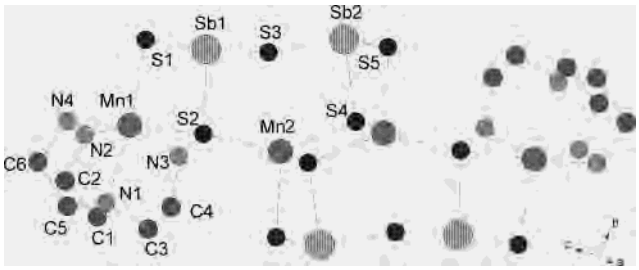

Figure 3. Crystal structure of **2** with labeling. Hydrogen atoms are omitted for clarity.

$Mn(2)S_4$. The two Sb atoms form typical SbS_3 trigonal pyramids. The structure of **2** is formed by the interconnection of these primary building units. The $Sb(1)S_3$ unit shares a common edge with the $Mn(1)N_4S_2$ octahedron to form an almost planar four-membered ring, $Mn(1)Sb(1)S_2$ (mean deviation from the best plane 0.0137 Å). Further condensation of the $Sb(1)S_3$ unit occurs via common corners with the $Sb(2)S_3$ pyramid and the $Mn(2)S_4$ tetrahedron. In addition, the $Mn(2)S_4$ tetrahedron and the $Sb(2)S_3$ pyramid have a common corner (S(4)), yielding a puckered six-membered heteroring ($Mn(2)Sb_2S_3$). The remaining part of the structure is generated by the center of inversion, and three further four-membered rings are formed. The mean deviation from the best plane for $Mn(2a)Sb(2)S_2$ is 0.1511 Å. The angle between $Mn(1)Sb(1)S_2$ and $Mn(2a)Sb(2)S_2$ is about 76.7°.

Some special features of $[Mn(tren)]_2Mn_2Sb_4S_{10}$ should be highlighted here: The S(2) atom is connected to three metal atoms (two Mn atoms and one Sb atom). Five four-membered heterorings and a six-membered heteroring are essential parts of the structure. In addition, neglecting the organic ligands, the structure consists of a $[Mn_2Sb_4S_{10}]$ core formed by the interconnection of the MnS_4 tetrahedra and the SbS_3 pyramids. This core may be viewed as a complex tetradentate ligand which is bound to two further Mn^{2+} ions, and such a manganese(II)−thioantimonate(III) core is very unusual and has never been reported before.

The Mn−N bond lengths range from 2.243(2) to 2.326(2) Å, with the longer bonds being in *trans* positions to the Mn−S bonds. The Mn(1)−S distances are very different:

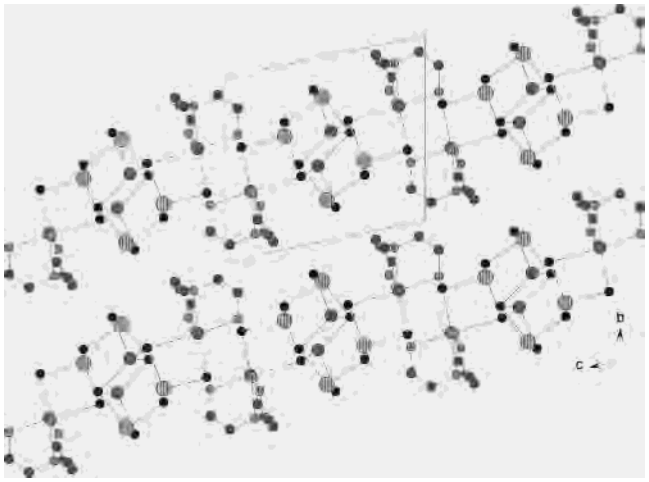

Figure 4. Arrangement of the $[Mn(tren)]_2Mn_2Sb_4S_{10}$ molecules in the structure. The H atoms and disordered C atoms are omitted for clarity.

2.4805(9) Å for Mn(1)−S(1) and 2.836(1) Å for Mn(1)−S(2). The S(2) atom is located in the distorted rectangular plane of the octahedron, and a shorter Mn(1)−S(2) bond has several consequences. The interatomic separation between S(2) and N(2) would be shortened, leading to repulsive interactions, and the Mn(2)−S(2) bond length would be enlarged to weaken this bond (Table 2, Figure 3). The Mn(2)−S bonds have distances 2.4693(9)−2.569(1) Å similar with the reported distances for interconnected MnS_4 tetrahedra.[52−54] The $[Mn(tren)]_2Mn_2Sb_4S_{10}$ molecules are stacked along [001] in a way that a layerlike arrangement is formed (Figure 4). Several relatively short intermolecular S···N separations may be regarded as weak hydrogen interactions (N−H···S distances between 2.501(3) and 2.7879(5) Å).

The Sb−S bond lengths are between 2.365(1) and 2.4831(1) Å, with S−Sb−S angles ranging from 91.73(4)° to 97.19(4)° both being in agreement with the data reported in the literature.

Thermoanalytical Investigations. On heating compound **1** at 4 °C/min to 350 °C, two strong endothermic events are observed at peak temperatures of about $T_{p1} = 233$ °C and $T_{p2} = 298$ °C in the DTA curve. They are accompanied by three steps in the TG curve (Figure 5). The total mass loss amounts to 27.2%. In the gray residue, elemental Sb, Sb_2S_3, and MnS were identified with XRD. Small amounts of organic residue were also found (CHN_{sum} 2.7%). The mass change during the first step suggests that the tren molecule is emitted in a well-defined way. To support this assumption, MS spectra were measured simultaneously during the thermal decomposition reactions. In agreement with our assumption up to 270 °C the fragment of tris(2-aminoethyl)amine ($m/z = 99$) could be detected. To acquire more information about this well-defined emission of one tren molecule in another run, the DTA−TG experiment was stopped after the first step. The X-ray powder pattern of the green-colored inter-

(52) Bronger, W.; Böttcher, P. *Z. Anorg. Allg. Chem.* **1972**, *390*, 1.
(53) Bronger, W.; Balk-Hardtdegen, H.; Schmitz, D. *Z. Anorg. Allg. Chem.* **1989**, *574*, 99.
(54) Bronger, W.; Böhmer, M.; Schmitz, D. *Z. Anorg. Allg. Chem.* **2000**, *626*, 6.

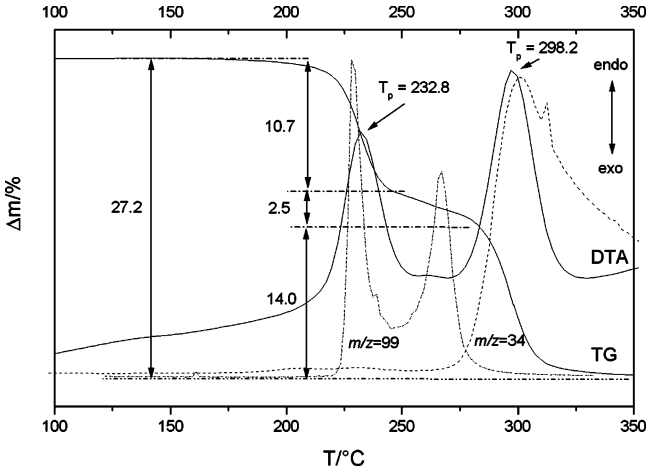

Figure 5. DTA, TG, and MS curves for $[Mn(tren)]_2Sb_2S_5$ (T_p = peak temperature; m/z = 34 (H_2S); m/z = 99 (tren)).

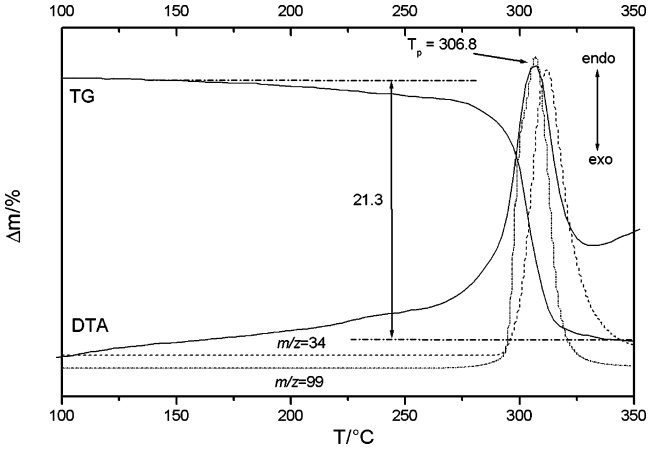

Figure 6. DTA, TG, and MS curves for $[Mn(tren)]_2Mn_2Sb_4S_{10}$ (T_p = peak temperature; m/z = 34 (H_2S); m/z = 99 (tren)).

mediate showed the reflections of compound **2** together with some weak reflections of elemental Sb. According to the MS data during the second decomposition, tren and H_2S are released (Figure 5). Therefore, we suggest that $[Mn(tren)]_2Sb_2S_5$ decomposes during the first step in the following way: $2[Mn(tren)]_2Sb_2S_5 \rightarrow [Mn(tren)]_2Mn_2Sb_4S_{10} + 2tren$. An interesting structural aspect is that the structure of **2** can be constructed using two $[Mn(tren)]MnSb_2S_5$ fragments which in turn may be obtained by the removal of one tren molecule from compound **1**. We note that the thermal transformation of compound **1** in **2** is not complete because elemental Sb is formed during the reaction.

Figure 6 shows the thermal decomposition of $[Mn(tren)]_2Mn_2Sb_4S_{10}$ at 4 °C/min until 350 °C. One strong endothermic event occurs at T_p = 307 °C. The experimental mass loss of 21.3% is in agreement with that expected for the removal of both tren ligands ($-\Delta m(tren)_{theo}$ = 22.2%). Additional mass spectroscopy demonstrates that the thermal decomposition of **2** is accompanied by the emission of tren and H_2S. In the gray residue, elemental Sb, Sb_2S_3, and MnS could identified with XRD and small amounts of organic residues were also found (CHN_{sum} 2.4%). Formally, the reaction can be described as $[Mn(tren)]_2Mn_2Sb_4S_{10} \rightarrow 4MnS + 3Sb + Sb_2S_3 + 3H_2S + 2tren$. We stress here that the thermal decomposition is complex due to redox reactions leading to the formation of elemental Sb.

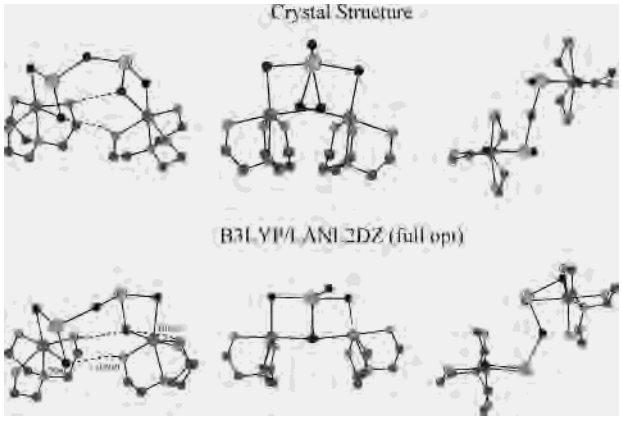

Figure 7. Comparison of the crystal structure (top) and the fully optimized structure (B3LYP/LANL2DZ) (bottom) of $[Mn(tren)]_2Sb_2S_5$. Hydrogen atoms involved in hydrogen bridges are shown as white spheres; all others are omitted for clarity.

Table 3. Comparison of Experimental and Calculated Geometric Parameters of $[Mn(tren)]_2Sb_2S_5$

param	X-ray[a]	opt[a]	param	X-ray[a]	opt[a]
Sb−S(1)	2.3980	2.514	Sb−S3−Sb[b]	134	123
Sb−S(2)	2.3589	2.553	hydrogen bonds		
Sb−S(3)	2.4725	2.579	H2N(2)−S(2)	3.077	2.64
Mn−S(1)	2.5006	2.537	H1N(3)−S(2)	2.670	2.54
Mn−S(2)	2.7036	2.658	H2N(2)[b]−S(2)[b]	2.541	2.36
Sb[b]−S(1)[b]	2.3980	2.546	H1N(3)[b]−S(2)[b]	2.670	2.47
Sb[b]−S(2)[b]	2.3589	2.500			
Sb[b]−S(3)	2.4725	2.627			
Mn[b]−S(1)[b]	2.5006	2.689			
Mn[b]−S(2)[b]	2.7036	2.570			

[a] Bond lengths in angstroms, angles in degrees. [b] Symmetry code $1 - x, y, 0.5 - z$.

Synthetic Aspects. On the basis of the results of the thermal decomposition reaction of compound **1**, the amine-poorer compound $[Mn(tren)]_2Mn_2Sb_4S_{10}$ (50 mg, 0.038 mmol) was used as the source in a solvothermal synthesis by applying 2 mL of tren and heating the mixture at 140 °C. After 14 days compound **1** was obtained in a good yield as a crystalline powder along with an unknown crystalline product.

Density Functional Calculations. The obtained structure of $[Mn(tren)]_2Sb_2S_5$ from DFT calculations is shown in Figure 7, right, and key structural parameters are compared to experimental parameters in Table 3. The overall structure calculated with DFT is quite similar to the experimentally determined one (Figure 7, left). Bond lengths of the $Mn_2Sb_2S_5$ subunit are in general obtained about 0.1 Å too long, which is not unusual for heavy atoms in nonrelativistic calculations. In the crystal structure, the two $MnSbS_2$ planes (MnSbS(1)S(2) and the symmetry-related plane in Figure 7) are planar and parallel to each other, resulting in an effective C_2 symmetry of the molecule (vide supra). In contrast, the calculated structure is only of C_1 symmetry (Experimental Section). This is due to the formation of new hydrogen bridges in the gas phase as indicated in Table 3 that lead to a distortion of the structure. In particular, the Mn(a)Sb(a)S(1a)S(2a) square is somewhat distorted from planarity,

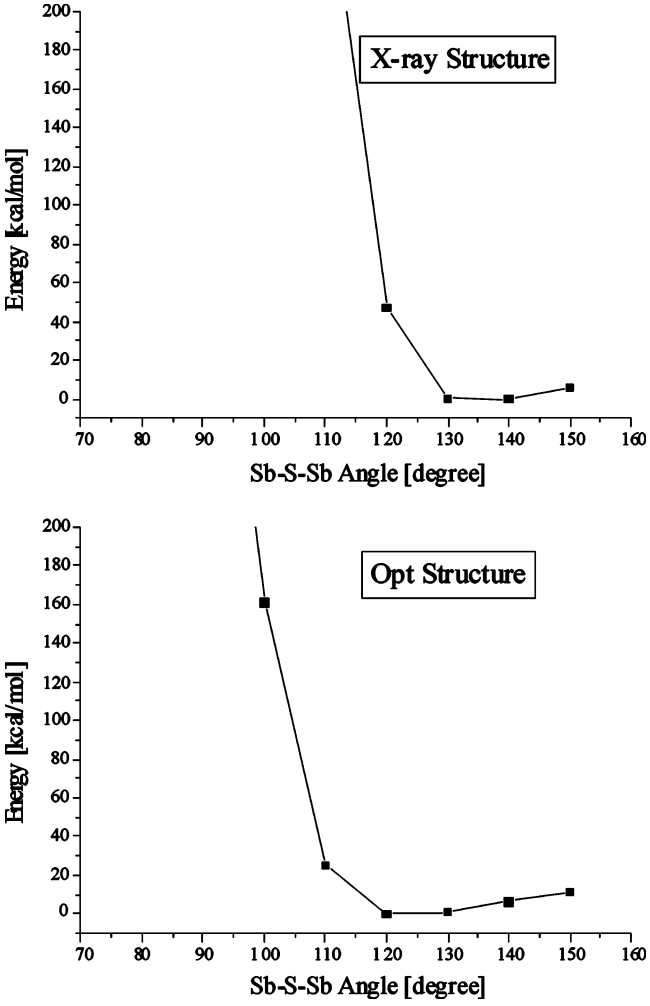

Figure 8. PES scans along the central Sb−S−Sb angle of $[Mn(tren)]_2Sb_2S_5$ for the crystal structure (top) and the fully optimized structure (bottom).

allowing the H2N(2)−S(2a) bridge to become extremely short (only 2.36 Å). This leads to a more open structure in the calculation (see Figure 7) as compared to experiment. Correspondingly, the Sb−S(3)−Sb(a) angle is reduced from 134° in the crystal structure to 123° in the calculation. This observation leads to the hypothesis that the large value of the Sb−S(3)−Sb(a) angle in compound **1** is related to the steric demand of the coordinated Mn(tren) subunit. To quantitatively estimate the energetics along the Sb−S(3)−Sb(a) coordinate, restricted PES scans have been performed for both the experimental and the calculated structures of $[Mn(tren)]_2Sb_2S_5$. Importantly, the PES for the crystal structure presented in Figure 8 shows that an Sb−S(3)−Sb(a) angle of 130−140° represents the actual energy minimum along this coordinate when all other geometric parameters are fixed. This is in very good agreement with the experimental value of 134°. Furthermore, the energy required for an enlargement of this angle to even 150° is still below 10 kcal/mol, which shows that this is an energetically soft coordinate. A decrease of the Sb−S(3)−Sb(a) angle below 130° is very unfavorable due to steric interactions between the two Mn(tren) subunits. The PES for the optimized structure is qualitatively identical (Figure 8), but the minimum is shifted to 123° in accordance with the more open geometry of the complex. To further explore the relationship between the Sb−S(3)−Sb(a) angle and the steric demand of the coordinated metal fragment, calculations have been performed on smaller, hypothetical systems. Geometry optimization of the sterically less crowded model $[Ni(NH_3)_2]_2Sb_2S_5$ leads to an overall structure that is comparable to $[Mn(tren)]_2Sb_2S_5$, but with an Sb−S−Sb angle of only 113°. This further supports the conclusion that the large value of the Sb−S−Sb coordinate in $[Mn(tren)]_2Sb_2S_5$ is due to steric strain. It also shows that the overall geometric structure of $[TM(L)]_2Sb_2S_5$ complexes (TM = transition metal; L = ligand(s)) as shown in Figure 7 is independent of the paramagnetism of Mn(II). The obtained structure of $[Ni(NH_3)_2]_2Sb_2S_5$ shows severe distortions due to strong hydrogen bonds between the terminal (negatively charged) sulfur atoms of the $[Sb_2S_5]^{4-}$ subunit and NH_3 groups coordinated to Ni. To further explore this point, calculations have been performed on the model compound $[Ni(tma)_2]_2Sb_2S_5$, where no such hydrogen bonds can be formed. Indeed, this leads to a much more open structure where the $Ni(tma)_2$ subunits are rotated away from each other and the Sb−S−Sb angle decreases further to 103°.

Conclusions

The major aim of our work is the understanding of the influence of different parameters which determine the product formation under solvothermal conditions. In addition, the structure−property relationship is another important part of our investigations. The final goal of the work is the optimization of the syntheses to reach a state where a more directed synthesis of thioantimonates(III) is possible. In the present paper we demonstrated that the solvothermal route allows the preparation of TM^{n+}-containing thioantimonates(III). Furthermore, we showed that the directed thermal decomposition of a suitable precursor material such as $[Mn(tren)]_2Sb_2S_5$ is a new synthetic approach in thioantimonate(III) chemistry. It must be noted that normally the starting thioantimonates(III) are fully destroyed during such thermal reactions. Hence, the observation that a well-crystallized new compound is formed by applying the directed thermal decomposition is unique in the field of thioantimonate(III) chemistry. In further experiments we presented evidence that the product of the thermal reaction can be used as a starting material for the synthesis of thioantimonate(III) compounds. In the present case the solvothermal treatment of $[Mn(tren)]_2Mn_2Sb_4S_{10}$ with tren leads to a full conversion into the starting compound $[Mn(tren)]_2Sb_2S_5$. This is the first example that even complex thioantimonates(III) can be used as sources for the synthesis of new compounds. Further experiments are under way to find suitable new starting compounds for the synthesis of thioantimonates with a high Mn:Sb ratio.

In the theoretical calculations using crystal structures of several $[TM(L)]_2Sb_2S_5$ complexes (vide supra), evidence is presented that the structure obtained for $[Mn(tren)]_2Sb_2S_5$ represents a general structural motif for such $[TM(L)]_2Sb_2S_5$ systems. This is due to the formation of strong hydrogen

bonds, which form a bridge between a Mn(tren) unit and an opposed sulfur.

Acknowledgment. This work has been supported by the State of Schleswig-Holstein and the Deutsche Forschungsgemeinschaft (DFG). We also thank Inke Jess for the acquisition of the single-crystal data and Jan Greve for the thermal measurements.

Supporting Information Available: Tables of atomic coordinates, isotropic and anisotropic displacement parameters, and full bond lengths and angles including details of the structure determination. This material is available free of charge via the Internet at http://pubs.acs.org.

IC034970+